Flagellar dynamics reveal large fluctuations and kinetic limit in the *Escherichia coli* chemotaxis network

Roshni Bano[1,3], Patrick Mears[2,3], Ido Golding[1,2,3], Yann R. Chemla[1,2,3,*]

[1]*Center for Biophysics and Quantitative Biology, University of Illinois, Urbana-Champaign*

[2]*Department of Physics, University of Illinois, Urbana-Champaign*

[3]*Center for the Physics of Living Cells, University of Illinois, Urbana-Champaign*

*For correspondence: ychemla@illinois.edu

Classification

Major Category: Biological Sciences

Minor Category: Biophysics and Computational Biology

Keywords

Bacterial chemotaxis, noise, CheY-P fluctuations, single cell, optical tweezers

Author Contributions

YRC supervised the project. YRC, IG, and PM conceived the experimental method. RB and PM performed the experiments. YRC and RB developed the analysis. RB performed the analysis and numerical simulations. YRC derived the analytical model with IG. RB and YRC wrote the manuscript with inputs from IG.

This PDF file includes:

Main Text, Figures 1 to 5

Abstract

Biochemical signaling networks allow living cells to adapt to a changing environment, but these networks must cope with unavoidable number fluctuations ("noise") in their molecular constituents. *Escherichia coli* chemotaxis, by which bacteria modulate their random run/tumble swimming pattern to navigate their environment, is a paradigm for the role of noise in cell signaling. The key signaling protein, CheY, when activated by (reversible) phosphorylation, causes a switch in the rotational direction of the flagellar motors propelling the cell, leading to tumbling. CheY-P concentration, [CheY-P], is thus a measure of the chemotaxis network's output, and temporal fluctuations in [CheY-P] provide a proxy for network noise. However, measuring these fluctuations in the single cell, at the relevant timescale of individual run and tumble events, remains a challenge. Here we quantify the short-timescale (0.5-5 s) fluctuations in [CheY-P] from the switching dynamics of individual flagella, observed using time-resolved fluorescence microscopy of optically trapped *E. coli* cells. This approach reveals large [CheY-P] fluctuations at steady state, which may play a critical role in driving flagellar switching and cell tumbling. A stochastic theoretical model, inspired by work on gene expression noise, points to CheY activation occurring in bursts, driving the large [CheY-P] fluctuations. When the network is stimulated chemically to higher activity, we observe a dramatic decrease in [CheY-P] fluctuations. Our stochastic model shows that an intrinsic kinetic ceiling on network activity places an upper limit on [CheY-P], which when encountered suppresses its fluctuations. This limit may also prevent cells from tumbling unproductively in steep gradients.

Significance Statement

Bacteria use intracellular signaling networks to navigate and adapt to their changing environment. These networks must cope with fluctuations in their molecular constituents, but the role this noise plays in cell behavior is not well understood. Here, we present a novel approach to quantify network noise in individual *Escherichia coli* cells. Our measurements show that the network exhibits larger-than-expected fluctuations when operating at a steady state; these fluctuations decrease dramatically when the network is activated by a chemical stimulus. A model inspired by gene expression noise studies recapitulates our findings and suggests that large fluctuations are driven by 'bursts' in signaling, drawing a parallel between the operating principles of gene regulatory and protein signaling networks.

Main Text

Introduction

A common feature of living organisms is their ability to sense environmental signals and respond to these signals by modifying their behavior. This ability is enabled by signal transduction, which converts environmental inputs into behavioral outputs[1]. Studies have shown that signaling networks must operate in the presence of noise not only in their inputs but also in the circuit components themselves[2,3]. Until recently, it was thought that signaling networks had evolved to be robust against undesirable noise[4–7]. More recent studies have shifted to understanding the role of noise in regulating and fine-tuning biological function[8,9]. For example, noise resulting from transcription/translation has been measured precisely and shown to play a critical role in networks for gene expression and regulation[10–12]. In contrast, studying noise resulting from signaling networks at the post-translation level has proven more challenging.

One extensively studied signaling system is the chemotaxis network of *E. coli*, which cells use to navigate their environment[13–17]. *E. coli* cells swim in a random walk consisting of "runs"—during which their flagella rotate counter-clockwise (CCW)—and "tumbles"—during which one or more flagella rotate clockwise (CW)[18–21]. Changing environmental conditions are sensed through a two-component signaling system comprising receptors that bind extracellular ligands and a kinase, CheA, that transfers its phosphoryl group onto downstream effectors[22]. The response regulator, CheY, when phosphorylated by the receptor kinase complex to CheY-P, binds to the flagellar motor and increases the probability of CW motor rotation[23–25]. The phosphatase CheZ carries out the opposite reaction, maintaining a dynamic equilibrium between CheY and

CheY-P (**Fig. 1a**)[26,27]. Additionally, the methyltransferase CheR and the methylesterase CheB covalently modify receptors, and the resulting modulation of CheA activity affects CheY-P levels over the long timescales (>10 s) of chemotactic adaptation[28–30]. While the population averaged relationships between these signaling protein concentrations and cellular motility in *E. coli* are now well understood[13–16,24], the role of fluctuations in protein concentrations in modulating cell behavior remains comparatively unexplored.

The intracellular CheY-P concentration, [CheY-P], is a dynamic indicator of the cell's environment and determines its trajectory of motion. Thus, [CheY-P] fluctuations are the primary indicator of noise upstream in the signaling network and affect downstream behavior. Cluzel et al. showed that the motor CW bias, the probability of CW rotation of a single flagellar motor, depends on the intracellular [CheY-P] in a sigmoidal manner[25]. Thus, the cell's swimming behavior is sensitive to small temporal fluctuations in [CheY-P] (**Fig. 1b, i-iii**). Noise due to CheY-P fluctuations was first inferred by Korobkova et al.[31] from long-term measurements of individual rotating flagellar motors, where larger-than-expected noise in the motor CW bias was attributed to methylation/demethylation dynamics of CheR/CheB over long timescales (10s of seconds). Recently, single-cell measurements probing intracellular [CheY-P] using fluorescent reporters revealed a potential new source of noise arising from the dynamics of the receptor kinase complex itself[32,33]. Noise in the *E. coli* chemotaxis signaling network is thought to have functional consequences for sensing and navigation in complex natural microenvironments. It has been proposed to allow cells to sample 3D space more effectively[31,34], enhance chemotactic drift up a gradient[35–37], and synchronize flagellar switching to mitigate differences in swimming behavior among cells with different numbers of flagella[38,39].

Here, we use optical trapping coupled with time-resolved fluorescence microscopy[39,40] to infer temporal [CheY-P] fluctuations from the statistics of flagellar switching in individual multi-flagellated *E. coli* cells. Unlike previous studies where fluctuations were studied over long timescales (>10 s)[31–33,41], we measure fluctuations at the short timescales of individual runs and tumbles (0.5-5 s; see **Materials and Methods**). Analyzing cells at steady state, we determine the single-cell distribution of [CheY-P], which reveals that the network is poised at a low CW bias, favoring CCW flagellar rotation/running, and that transient fluctuations in [CheY-P] drive CW flagellar rotation/tumbling. We also find that these fluctuations are significantly reduced upon applying a stimulus that increases CheA activity. A simple stochastic model in which noise in signaling arises from large, burst-like fluctuations in CheA activity recapitulates all of our experimental results and suggests that the decrease in CheY-P fluctuations upon stimulation is due to a kinetic ceiling on the CheA activity.

Results

Flagellar switching statistics reveal temporal [CheY-P] fluctuations

We inferred the temporal fluctuations in the intracellular CheY-P concentration from the dynamics of flagellar switching in individual cells. We imaged fluorescently labeled flagella on individual, swimming cells to determine their CCW/CW rotation state, using an optical trapping assay described previously[39,40,42] (see **Supplementary Information**). Briefly, *E. coli* cells were injected into a laminar flow chamber containing two parallel channels. A single cell was captured using a dual beam optical trap from one channel containing many cells (labeled “cells” in **Fig. 1c**) and moved for observation to a second channel containing no other cells (labeled “blank” in **Fig.**

1c). The light scattered by the optically trapped cell was used to monitor the run/tumble swimming behavior as described previously (data not shown, see Ref. [39]). Simultaneously, high-speed, epi-fluorescent stroboscopic imaging[39] was used to monitor the rotation state of all the individual flagella on the cell at high temporal resolution (0.1 s) and long-time duration (typically ~30-40 s, until the flagella photobleached) (**Fig. 1d,** top). Following Darnton et al.[21] and our previous work[39], the CCW/CW rotation state of each flagellum was visually identified by its different helical waveforms (see **Supplementary Information**).

We next inferred the distribution of [CheY-P], making use of the statistics of switching in multi-flagellated cells. For a cell with N flagellar motors, the probability that n_{cw} rotate in a CW direction, $p_N(n_{cw})$, is equal to (see **Supplementary Information**):

$$p_N(n_{cw}) = \int_0^1 dc\, p_N(n_{cw} \mid c) p(c)\,, \tag{1}$$

where c is the instantaneous motor CW bias, or probability that any one motor is CW, $p_N(n_{cw} \mid c)$ is the conditional probability that n_{cw} out of N motors are in the CW state given a certain c, and $p(c)$ is the distribution of CW biases (**Fig. 1b, iii**). Given the finding that flagellar motors switch independently of each other[39], $p_N(n_{cw} \mid c)$ is given by the binomial distribution:

$$p_N(n_{cw} \mid c) = \binom{N}{n_{cw}} c^{n_{cw}} (1-c)^{N-n_{cw}}\,. \tag{2}$$

The motor CW bias c depends on the intracellular CheY-P concentration in a switch-like manner, customarily modeled by a sigmoidal Hill curve (**Fig. 1b, ii**)[25]:

$$c = \frac{y_P^H}{K^H + y_P^H}\,, \tag{3}$$

where $y_P \equiv$ [CheY-P]. Measurements from cell populations report a Hill coefficient $H = 10.3 \pm 1.1$[25] and a CheY-P concentration at 0.5 CW bias $K = 3.1$[25] ± 0.01[43] μM. Thus, Eq. (1) for $p_N(n_{cw})$ can be written in terms of [CheY-P]:

$$p_N(n_{cw}) = \int_0^{y_{\text{tot}}} dy_P \; p_N(n_{cw} \mid y_P) p(y_P) \,, \tag{4}$$

where y_{tot} is the total intracellular CheY concentration, reported to be 9.7 ± 0.4 μM for cells under growth conditions similar to ours[44] (see **Supplementary Information**). $p(y_P)$ is the distribution of [CheY-P] (**Fig. 1b, i**), and the conditional probability $p_N(n_{cw} \mid y_P)$ is obtained by combining Eq. (2) and (3) to yield:

$$p_N(n_{cw} \mid y_P) = \binom{N}{n_{cw}} \frac{y_P^{n_{cw} H}}{(K^H + y_P^H)^N} \,. \tag{5}$$

Since the conditional probability is known, Eq. (4) in principle allows one to connect the probability $p_N(n_{cw})$—which can be determined from measurements of the CCW/CW rotational state of each flagellum of a cell with N flagellar motors—to the distribution of [CheY-P], $p(y_P)$. (Eq. (1) can similarly be used to connect to the distribution of CW biases $p(c)$). In practice, solutions to Eqs. (1) and (4) are not unique, but one can show that an increasing number of moments of the distribution $p(c)$ are determined as N increases (see **Supplementary Information**). Thus, one expects that the distribution $p(c)$, and thus the distribution $p(y_P)$ which captures fluctuations in [CheY-P], can be estimated with increasing accuracy as N increases. Essentially, since each flagellar motor independently measures the intracellular level of CheY-P, the more motors a cell possesses, the better our estimate of the mean [CheY-P] and its fluctuations.

We note that while $p(c)$ is determined exactly from Eq. (1) with no additional input parameters, $p(y_P)$ requires values for the parameters y_{tot}, K, and H in Eqs. (4) and (5). Because the CW bias $c \approx 1$ when $y_P = y_{\mathrm{tot}}$ according to Eq. (3), the integral in Eq. (4) is insensitive to the exact value of y_{tot}. (Its upper limit can be replaced with ∞ with error <0.01%). However, $p(y_P)$ depends more strongly on K and H; for example, the [CheY-P] concentration y_P is determined only relative to K. Throughout, we assumed experimentally determined[25,43] values of K = 3.1 μM and H = 10.3 (see **Supplementary Information** for a more detailed discussion on the sensitivity to experimental parameters).

Figure 1 shows the workflow to determine $p(y_P)$ experimentally. Fluorescence tracking of the CCW/CW state of the individual flagella (**Fig. 1d,** middle) is represented as a time trace of the number of CW flagella (**Fig. 1d,** bottom). For a cell with N flagella, a histogram of this time trace was used to construct the probability distribution $p_N(n_{cw})$ that n_{cw} out of N flagella rotate CW (**Fig. 1e**, bottom**,** histogram). We determined the probability distribution $p_{fit}(y_P)$ (**Fig. 1e**, top) via the integral equation Eq. (4), using a trial distribution function and finding the parameters that generated the probability distribution $p_{N,fit}(n_{cw})$ (**Fig. 1e**, bottom, solid line) that best fitted the experimental distribution (see **Materials and Methods**). Below we show the results of this analysis for one choice of trial distribution function (see **Supplementary Information** for a discussion on alternate choices).

The chemotaxis network exhibits large [CheY-P] fluctuations at steady-state

We first applied the above approach to free-swimming (i.e. unstimulated) cells for which the chemotaxis network is in a steady state. Fluorescence tracking data of CCW/CW flagellar states

were obtained for cells of a strain wild-type for chemotaxis (HCB1660, henceforth referred to as "wild-type"; see **Supplementary Information**) with N = 2 to 5 flagella. Data traces tracking n_{cw} were pooled together from multiple cells with the same total number of flagella N to generate $p_N(n_{cw})$ (**Fig. 2a**, colored histograms). As we show below, pooling did not affect our results appreciably.

Since we did not expect the number of flagella to have an effect on fluctuations of the underlying network, we fitted the data globally, determining a single [CheY-P] distribution for all values of N. The best fit global [CheY-P] distribution, $p_{glofit}(y_P)$, is shown in **Fig. 2c** (gray solid curve) and the corresponding distributions of number of CW flagella, $p_{N,glofit}(n_{cw})$, are shown in **Fig. 2a** (gray solid lines). We also show the motor bias distribution $p_{glofit}(c)$ in **Fig. 2b**. We used the beta distribution (see **Supplementary Information**; Eq. (S12)) as a trial distribution function for $p_{glofit}(c)$ and Eq. (1) and Eq. (S8) to determine $p_{glofit}(y_P)$ (see **Materials and Methods**). The mean [CheY-P], $\mu_{y_p,glo}$, and the standard deviation, $\sigma_{y_p,glo}$, from this global fit were 2.2 ± 0.1 μM and 0.8 ± 0.1 μM, respectively. **Supp. Fig. 1** shows the estimated error in the best fit [CheY-P] distributions, as determined by bootstrap resampling (see **Materials and Methods**). Alternate choices of trial functions for $p_{fit}(y_P)$ did not change the mean and standard deviation appreciably, although some functions fit the data better than others (see **Supplementary Information**, **Supp. Fig. 2**, and **Supp. Table 3**). As a comparison, we also determined the [CheY-P] distribution $p_{fit}(y_P)$ and CW bias distribution $p_{fit}(c)$ separately for each set of cells with different number of flagella N (**Fig. 2c** and **2b**, colored solid curves), along with the best fit distribution of the number of CW flagella, $p_{N,fit}(n_{cw})$ (**Fig. 2a**, colored solid lines). Although the distributions $p_{N,fit}(n_{cw})$ were better fit for each individual N, the corresponding $p_{fit}(y_P)$ for each N were comparable to that obtained by a global

fit, as shown in **Fig. 2c** (see **Supp. Table 4**). The mean and standard deviation in [CheY-P] averaged over the separate fits, $<\mu_{y_p}>$ = 2.2 ± 0.2 μM and $<\sigma_{y_p}>$ = 0.71 ± 0.04 μM, were almost identical to those obtained by a global fit, indicating that a single global distribution describes the data across *N* and that the number of flagella does not affect network fluctuations measurably. The above analyses thus show that [CheY-P] fluctuations in free-swimming wild-type cells results in a coefficient of variation σ_{y_p}/μ_{y_p} = 0.3-0.4.

We carried out several tests to confirm that the width of the estimated [CheY-P] distribution resulted from noise in signal transduction. First, we applied our method of analysis to a strain that expresses the constitutively active mutant protein $CheY^{D13K}$, a mimic for CheY-P[24] (strain PM87, henceforth referred to as "CheY*"; see **Supplementary Information**). Since CheY in this strain is decoupled from the upstream network components and the concentration of $CheY^{D13K}$ is determined from gene expression levels, which should not fluctuate on the timescales of our experiments in nutrient-limited conditions[45], we expected to observe smaller fluctuations in [$CheY^{D13K}$] as compared to the wild-type strain. Repeating the above analysis, **Figures 2d**-**f** show the experimental distributions $p_N(n_{cw})$ along with all fit distributions. Values for the mean [$CheY^{D13K}$] and standard deviation from fits for each *N* and from a global fit are found in **Supp. Table 5**. The mean [CheY-P] is similar for both strains, and, as expected, fluctuations in the CheY* strain are much reduced compared to the wild-type strain, yielding a coefficient of variation of 0.15.

Second, we tested whether the width of the estimated [CheY-P] distribution could be due to cell-to-cell differences in mean [CheY-P] rather than fluctuations arising in signal transduction. To test the contribution of cell-to-cell variation, we determined the best fit [CheY-P] distributions

for individual cell traces (**Supp. Fig. 3** and **4**) and compared the wild-type and CheY* strains. As shown in **Fig. 3a** and **3b**, while the mean [CheY-P], μ_{y_p}, from individual cell distributions was similar for both strains, the coefficient of variation, σ_{y_p}/μ_{y_p}, was significantly smaller for the CheY* strain as compared to the wild-type strain ($p < 0.05$), as expected. Importantly, the coefficient of variation for individual wild-type cells averaged over N, $<\sigma_{y_p}/\mu_{y_p}> \approx 0.3$, was identical to that determined over the population. This indicates that cell-to-cell variation over the wild-type cell population does not contribute greatly to the observed width in the [CheY-P] distribution. In contrast, $<\sigma_{y^*}/\mu_{y^*}>$ was significantly smaller for individual cells of the CheY* strain, ~0.07, as compared to the population, 0.15. We suspect cell-to-cell $CheY^{D13K}$ expression differences may contribute to the estimated distributions in **Fig. 2d-f**. Nevertheless, our results show that we can attribute the width in the [CheY-P] distribution for wild-type cells to fluctuations in [CheY-P] due to signaling activity. Our estimate of CheY-P fluctuations in wild-type cells is consistent with a theoretically predicted lower bound of 20% of the mean, albeit based on long time scale measurements[46]. In comparison, recent measurements report noise in receptor kinase activity of ~40% of the mean[33], also at long time scales.

One interesting observation, comparing our estimated distribution $p(y_P)$ to the Hill curve relating CW bias to [CheY-P], Eq. (3) (**Fig. 2c**), is that the peak of the distribution resides at low CW biases, $c < 0.05$, corresponding to CCW flagellar rotation and running a majority of the time. CW rotation and tumbling thus result from fluctuations away from the peak, in the tail of the distribution at higher [CheY-P]. This finding contrasts with the conventional view that the network is poised near the midpoint of the Hill curve[36], i.e. with $p(y_P)$ sharply peaked near [CheY-P] $\approx K$, and suggests that fluctuations are a critical determinant of the tumbling frequency.

[CheY-P] fluctuations decrease upon stimulating the network to increase CW bias

Having characterized fluctuations in the chemotactic network in the steady state, we next investigated them in a network stimulated by a perturbation. In response to a stepwise change in chemical environment, the intracellular [CheY-P] changes rapidly, and then reverts to its steady-state value through adaptation[47–49]. Applying a large stepwise decrease in attractant leads to a transient increase in [CheY-P] and flagellar motor CW bias followed by a decrease to the steady state[42,50], allowing us to measure network fluctuations across the sensitive range of the motor CW bias vs. [CheY-P] curve, Eq. (3).

We measured the response of individual cells to a decrease in concentration of α-methyl-DL-aspartate (MeAsp), a non-metabolizable analog of L-aspartate[51] that acts as a chemoattractant[51,52]. We used a three-channel flow chamber (**Fig. 4a**) to observe the effect of a step-down from 1 to 0 mM MeAsp on individual optically trapped wild-type cells. The step-down was applied by quickly moving a trapped cell from the middle channel of the flow chamber containing 1 mM MeAsp (**Fig. 4a**; labeled "blank + attractant") to the top channel containing no MeAsp (labeled "blank"; see **Supplementary Information**). The run-tumble behavior of the cell was monitored pre- and post-stimulus via the optical traps (see **Supplementary Information**), whereas the flagellar rotation state was measured by fluorescence imaging only post-stimulus.

Figure 4b shows a representative measurement of a cell with 3 flagella undergoing a step-down stimulus at t = 0. In response, the cell exhibits the expected increase in tumbling immediately post-stimulus, followed by relaxation to the pre-stimulus steady state as the cell adapts (**Supp. Fig. 5**). As the probability of tumbling is directly related to the probability of CW flagellar rotation[39], n_{cw} measured by fluorescence imaging post-stimulus also relaxes to lower

values as the cell adapts (**Fig. 4b**, blue trace). Since the [CheY-P] distribution $p(y_P)$ is time-dependent in cells responding to a step-down, the time traces of n_{cw} for each cell were divided into time windows corresponding to 20% of the cell's adaptation time (**Fig. 4c**, colors corresponding to time window), over which the average tumble bias was constant to within ~10-20%. The best fit [CheY-P] distribution $p_{fit}(y_P)$ was estimated separately for each window (see **Supplementary Information** for more details on windowing). All data from cells with the same total number of flagella (in **Fig. 4c**, three representative cells with N = 3 flagella) were pooled in similarly constructed time windows and used to create histograms $p_N(n_{cw})$ at each time (**Fig. 4d**). $p_{fit}(y_P)$ corresponding to each time window was then found as described above (**Fig. 4e**, colored curves). Relative to unstimulated cells (**Fig. 4e**, gray curve for unstimulated wild-type cells with N = 3 flagella), the peak of the [CheY-P] distribution shifted to a higher value immediately after the stimulus, as expected for a step down. While we expected the standard deviation to increase as the mean [CheY-P] increased, the width of the [CheY-P] distribution instead decreased (**Fig. 4e**). We verified that the reduction in noise was due to a change in chemotaxis network dynamics after stimulation rather than due to windowing of the data; 4-s time windows of data traces of individual wild-type cells at steady-state did not have significantly narrower [CheY-P] distribution widths compared to full-length traces (see **Supp. Fig. 6**).

The time-dependent, post-stimulus mean μ_{y_p} and coefficient of variation σ_{y_p}/μ_{y_p} of [CheY-P] for cells with N = 2, 3, 4 flagella are shown in **Fig. 5a** and **5b** (colored filled circles), respectively. The corresponding steady-state mean and coefficient of variation obtained from **Fig. 2** are also plotted for reference (for $t < 0$, colored open circles). As expected, the trends are similar for cells with different numbers of flagella. Thus, we estimated these parameters from a fit to a global

[CheY-P] distribution across cells with different *N* for each time window (**Fig. 5a** and **5b**; gray filled circles; see **Materials and Methods**). Consistent with the distributions in **Fig. 4d**, the mean [CheY-P] increases immediately (to ~3 μM) in response to the step-down stimulus and relaxes toward its steady-state, pre-stimulus value as the cells adapt. At the same time, the coefficient of variation in [CheY-P] falls post-stimulus, then gradually increases toward the pre-stimulus value.

These results point to two interesting features. First, the mean [CheY-P] rises from a pre-stimulus steady state of ~2 μM to ~3 μM immediately after the step down (**Fig. 5a**). While the increase in [CheY-P] and the resulting increase in CW bias is expected for a step-down stimulus, it is smaller in magnitude than predicted by existing models[44,53]. Given the strength of the stimulus (from 1 to 0 mM [MeAsp]), these models predict a CW bias close to 1, corresponding to [CheY-P] >5 μM immediately post stimulus; instead, [CheY-P] remains near the midpoint of the CW bias vs. [CheY-P] curve, Eq. (3). Second, fluctuations are significantly reduced immediately after the stimulus is applied, decreasing from ~0.7 μM (or σ_{y_p}/μ_{y_p} = 0.3) pre-stimulus to as low as ~0.1 μM (or σ_{y_p}/μ_{y_p} = 0.05) post-stimulus (**Fig. 5b**). This value is as low as that measured in individual CheY* cells (**Fig. 3b**), suggesting that fluctuations in the network are largely suppressed when driven to high CW bias.

A stochastic model incorporating CheA activity fluctuations reproduces the experimental results

We next sought a stochastic model to describe our experimental results. The intracellular CheY-P is controlled by fast phosphorylation-dephosphorylation reactions,

$$\text{CheY} \underset{k_z}{\overset{k_A a}{\rightleftharpoons}} \text{CheY-P}\,, \tag{6}$$

in which the rate of CheY phosphorylation by the CheA-receptor complex is written as $k_A a$, where a is the probability that CheA is in its active state and k_A is the maximum phosphorylation rate[54,55], and in which k_Z is the rate of CheY-P dephosphorylation by the phosphatase CheZ. These rates are expected to be on the order of 10 s^{-1} [53–55]. We first determined if this set of reactions alone could generate the number fluctuations in CheY-P to reproduce the observed noise. Using the chemical master equation (CME), the following analytical solution for the coefficient of variation in [CheY-P] (see **Supplementary Information**) is obtained[56]:

$$\frac{\sigma_{y_P}}{\mu_{y_P}} = \sqrt{\frac{1}{\mu_{y_P} V_C}\left(1 - \frac{\mu_{y_P}}{y_{tot}}\right)}, \tag{7}$$

where the mean [CheY-P] is given by $\mu_{y_p} = y_{tot} k_A a / (k_A a + k_Z)$ and V_C is the *E. coli* cell volume, assumed to be 1.4 fL[57] ($V_C^{-1} \approx 1.2$ nM).

To compare this model to the experimental data, we plotted in **Fig. 5c** the coefficient of variation vs. the mean [CheY-P] for cells at steady state (open circles) and for stimulated cells (filled circles). While all of the experimental data trace one continuous curve, this curve differs from the model Eq. (7) in two significant ways. First, for low mean [CheY-P], Eq. (7) (dotted line in **Fig. 5c**) predicts a coefficient of variation σ_{y_p}/μ_{y_p} over an order of magnitude smaller than our experimentally determined value. Fundamentally, the low number fluctuations predicted from Eq. (7) are due to the large total number (~8,000) of CheY molecules in the cell. Matching our experimental data would require decreasing the number of CheY by over two orders of magnitude (equivalent to replacing V_C with a cell volume two orders of magnitude smaller in Eq. (7)). Although a recent study proposed that CheY sequestration at the cell poles where many

signaling proteins reside may limit the number of CheY-P participating in signaling[58], such a mechanism is unlikely to account for this discrepancy between Eq. (7) and our data.

Second, the dramatic decrease in coefficient of variation near μ_{y_p} = 3 μM, which results from the observed narrowing of the [CheY-P] distributions in stimulated cells (**Fig. 4e**), is not recapitulated in the model. Eq. (7) predicts a drop to zero at y_{tot} = 9.7 μM, when all of the CheY becomes phosphorylated. One possibility to account for these observations is a ceiling of ~3 μM on the amount of CheY available for phosphorylation, leading to a maximum [CheY-P] ≈ 3 μM and a reduction in the width of the [CheY-P] distribution at this concentration. To test this mechanism, we constructed a mutant *ΔcheZ* strain ("RB03"; see **Supplementary Information**) lacking the phosphatase CheZ, in which all the available CheY is expected to be phosphorylated. Replicating our flagellar imaging analysis from above with this strain yields a mean [CheY-P] of 5.3 ± 1.1 μM, corresponding to a CW bias close to 1 according to Eq. (3) (data not shown), higher than that observed following a step-down stimulus, ruling out such a mechanism.

An alternate, more plausible mechanism is that additional sources of noise contribute to the two-species model in Eq. (6). One such source is fluctuations in phosphorylation-dephosphorylation kinetics. Although Eq. (6) assumes constant rates, the activity of the CheA-receptor complex is thought to fluctuate over time[31,32]. To model CheA fluctuations, we modified Eq. (6) to allow CheA to interconvert between active and inactive states, leading to a fluctuating activity $a(t)$. Adapting the approach of Paulsson et al.[59,60], the following analytical solution for the coefficient of variation in [CheY-P] in the presence of CheA fluctuations is obtained (see **Supplementary Information**):

$$\frac{\sigma_{y_P}}{\mu_{y_P}} = \sqrt{\frac{1}{\mu_{y_P} V_C}\left(1 - \frac{\mu_{y_P}}{y_{tot}}\right)\left[1 + \langle b \rangle \left(1 - \frac{\mu_{y_P}}{\alpha y_{tot}}\right)\right]}, \tag{8}$$

where the factor in brackets represents the contribution of CheA activity fluctuations to CheY-P noise. Here $\langle b \rangle$ denotes the number of new CheY-P generated during the time periods when CheA is active. The factor $\alpha \equiv k_A / (k_A + k_Z)$ is the fraction of CheY that is phosphorylated when all CheA are active, i.e. when the activity a = 1.

This model recapitulates the features of the data well; **Fig. 5c** shows a fit to Eq. (8) (dashed line) with parameters $\langle b \rangle$ = 580 ± 150 and α = 0.30 ± 0.01 (R^2 = 0.6; errors represent 95% confidence interval). Analogous to "burst size" in stochastic gene expression[61,62], $\langle b \rangle$ increases number fluctuations in CheY-P, matching the data. The parameter α represents the fact that the contribution of CheA fluctuations to CheY-P noise must go to zero when a = 1, which occurs in **Fig. 5c** at a mean [CheY-P] of $\mu_{y_P} = \alpha y_{tot} \approx 3$ μM. The value of α points to a kinetic ceiling on CheA-receptor complexes of $k_A = 0.43 k_Z$, or 13 s^{-1} assuming a constant CheY-P dephosphorylation rate of k_Z = 30 s^{-1}, within the reported range[53–55]. A maximum rate k_A = 13 s^{-1} is consistent with reported values of the CheA auto-phosphorylation rate, the rate-limiting step for CheY phosphorylation[35,53–55]. (We note that in the *ΔcheZ* strain, the kinetic ceiling on k_A would not cap [CheY-P] since k_Z = 0.) To confirm these analytical results, we also carried out stochastic simulations of Eq. (6) (see **Supplementary Information**). For simplicity we assumed a constant CheY-P dephosphorylation rate of k_Z = 30 s^{-1} and sampled the CheA activity from a gamma distribution with mean and variance chosen to recapitulate the experimental results in **Fig. 5c**.

Simulation results were consistent with our analytical results and our model of a kinetic ceiling on CheA activity (**Supp. Fig. 7**).

Discussion

In this work we demonstrate a new approach for inferring fluctuations in [CheY-P] based on the statistics of flagellar switching in multi-flagellated *E. coli* cells. One advantage of this approach is that its accuracy in quantifying network noise does not depend on temporal averaging, limiting previous measurements to long time scales[31,33], but instead relies on multiple flagellar motors making independent simultaneous "measurements" of intracellular CheY-P levels. This feature allows us to measure short-timescale [CheY-P] noise (0.5-5 s). In **Supp. Fig. 6**, we show that for individual wild-type cells at steady state, the mean μ_{y_p} and coefficient of variation σ_{y_p}/μ_{y_p} measured over non-overlapping 4-s windows show no significant differences from those for full-length individual traces (20-30 s) ($p > 0.01$), confirming that we indeed measure short-timescale [CheY-P] fluctuations. Short time scale measurements also allow us to track the time evolution of signaling noise in cells undergoing adaptation.

Previous single-cell measurements of flagellar rotation by bead tracking[31,41] and of CheA activity using fluorescent reporters[32,33] have reported long-term noise in the chemotaxis network attributed to CheR-CheB methylation-demethylation dynamics[31] and, recently, new sources such as receptor clustering and other dynamics[32,33]. Since these fluctuations occur over the long time scales of chemotactic adaptation (>10 s), we suspect that the source of CheY-P noise in our data, modeled successfully by the CheA activity fluctuations in Eq. (8) (**Fig. 5c**), may be distinct. Recently, Terasawa et al.[38] proposed that waves of CheA activity cause transient increases in

[CheY-P] over short timescales (≤ 1 s), as evinced by their observations of correlated flagellar switching. Our data and model appear to be consistent with this mechanism, with the "burst size" $\langle b \rangle$ in Eq. (8) representing such waves in activity. Our fit parameters indicate that ~8% of all CheY are phosphorylated during such events.

In contrast to prior fluorescence-based studies, which determine changes in CheA activity relative to a baseline[32,33], we determine noise parameters in terms of absolute CheY-P concentration, which allows for direct comparison to theoretical models. However, one limit is that our estimate of $p(y_P)$ depends on the relation between CW bias and [CheY-P], modeled by the Hill curve in Eq. (3). While we have assumed throughout values of H = 10.3 and K = 3.1 μM in Eq. (3), any changes to these parameters affects our inference of [CheY-P] fluctuations from flagellar switching statistics. Several recent studies have pointed to mechanisms affecting the values of these parameters[43,63]. We discuss these considerations and our sensitivity to H and K at length in the **Supplementary Information**. Nevertheless, the relative differences between various [CheY-P] distributions—such as between the wild type cells and the CheY* mutant, or between different time points in adapting cells—still remain significant. Thus, the trends in our results remain valid independent of parameter values.

The noise characteristics of the chemotaxis network revealed in our measurements may have functional consequences. Our findings suggest that short-timescale [CheY-P] fluctuations are critical drivers for CW flagellar rotation/tumbling in *E. coli*. Our experimentally determined mean [CheY-P] of 2.2 μM restricts the cell to a CW bias <0.05, corresponding to running the majority of the time. We envision that transient increases in [CheY-P], driven by waves of phosphorylation by the receptor kinase complex[38], increases the CW bias to generate tumbles. In previous work,

it was proposed that such short-timescale [CheY-P] fluctuations act to synchronize flagellar switching[38,39], which was shown to make swimming behavior robust to variation in flagella number[39]. *E. coli* has been proposed to exploit long-timescale [CheY-P] fluctuations to explore larger volumes of space[31,34] and to increase drift speeds, enhancing migration along increasing attractant gradients[35–37]. It is possible that shorter-timescale network noise characteristics could similarly influence chemotactic efficiency. Lastly, the kinetic ceiling in receptor kinase activity which restricts CheY-P fluctuations when the mean [CheY-P] increases could prevent CheY-P concentrations from saturating and leading to continuous and unproductive CW flagellar rotation/tumbling. Such behavior could result in increased *E. coli* swimming efficiency down steep decreases in attractant concentration, as likely found in natural environments.

Materials and Methods

Experiments were performed with the *E. coli* strains HCB1660 (wild-type)[64], PM87 (CheY*)[39] and RB03 (this work, see **Supplementary Information**). All these strains contained the mutant $FliC^{S219C}$ protein which allows fluorescent labelling of flagella[64]. Following our previous work[39], we fluorescently labelled flagella of *E. coli* cells grown in tryptone broth (TB) to OD_{600} ~0.4-0.5 (after dilution from an overnight culture) and resuspended in motility buffer[21]. Labelled cells were diluted in trap motility buffer (TMB[42]: 70 mM NaCl, 100 mM Tris-Cl, 2% [wt/vol] glucose, with 0.1 mM methionine and an oxygen-scavenging system [290 µg ml^{-1} pyranose oxidase and 65 µg ml^{-1} catalase]) and injected into a flow chamber.

Experiments were performed with a dual-trap optical tweezers instrument combined with epi-fluorescence slim-field imaging, developed and described by Mears et al.[39]. Custom-built microfluidic chambers (**Fig. 1c** and **4a**) were used to perform motility assays coupled with fluorescence imaging of labelled flagella on individual trapped cells. Fluorescently labeled flagella of individual trapped cells were imaged at 100 frames per second to record movies, typically for ~30-40 s until the flagella photobleached. For each movie, Clockwise (CW)/Counter Clockwise (CCW) states, visually identifiable by their different helical waveforms, were assigned manually to each flagellum over a 100 ms time window. Waveform transitions take less than ~0.5 s to propagate through flagella.

We extracted [CheY-P] distributions from flagellar imaging movies of individual cells by determining the fraction of the time that n_{cw} out of a total of N flagella rotated CW, $p_{N,obs}(n_{cw})$, where n_{cw} = 0, 1… N. For each N, [CheY-P] distributions were estimated separately by assuming a

trial distribution function p_{fit} (of either motor bias c or [CheY-P] y_P), evaluating $p_{N,fit}(n_{cw})$ using the integral in Eq. (1) or (4), and finding parameters for p_{fit} that best fit the experimentally observed distribution $p_{N,obs}(n_{cw})$ using a χ^2 minimization routine. We estimated errors by bootstrapping over individual cell time traces and running the χ^2 minimization routine. Additionally, we estimated a single global [CheY-P] distribution that fit all datasets across all N.

For trapped cells experiencing a step-down in MeAsp, each individual cell time trace for n_{cw} was divided into non-overlapping windows and n_{cw} for multiple cells with the same total number of flagella N were pooled in each time window. The time-dependent histogram $p_{N,obs}(n_{cw},t)$ was constructed and the time-dependent [CheY-P] distribution $p_{fit}(y_P,t)$, along with the associated error, was determined for each time window. For each window, we also calculated a global [CheY-P] distribution across all N.

We used a stochastic chemical kinetics approach to model CheY-P fluctuations. We chose the simplest possible scenario, considering only the CheY phosphorylation and CheY-P dephosphorylation reactions, Eq. (6), and used a chemical master equation (CME) to determine the mean and standard deviation of the number/concentration of CheY-P molecules. We considered two phosphorylation-dephosphorylation reaction schemes: the first, where CheA activity remained constant, leading to Eq. (7), and the second, where CheA activity fluctuated, leading to Eq. (8). To validate these analytical results, we also performed numerical simulations. A detailed description of the experiments, analysis and modeling are provided in the **Supplementary Information**.

Acknowledgements

We are grateful to David Bianchi and Zaida Luthey-Schulten for helping us run simulations using their custom-built software package Lattice Microbes. We are thankful to Tom Kuhlman for guiding us through the process of molecular cloning, and to Howard Berg for providing bacterial strains. Finally, we thank members of the Chemla laboratory for scientific discussions and Christopher Rao for providing comments on the manuscript. Work in the Chemla and Golding labs is supported by National Science Foundation Physics Frontiers Center (PFC) "Center for the Physics of Living Cells" (CPLC) PHY-1430124. Work in the Golding lab is supported by the National Institutes of Health grant no. R01 GM082837.

References

1. Lim WA, Mayer B., P. T. *Cell Signaling*. (Garland Science, 2014).

2. Mcadams, H. H. & Arkin, A. Stochastic mechanisms in gene expression. *Proc. Natl. Acad. Sci. U. S. A.* **94**, 814–819 (1997).

3. Allen, C. & Stevens, C. F. An evaluation of causes for unreliability of synaptic transmission. *Proc. Natl. Acad. Sci. U. S. A.* **91**, 10380–10383 (1994).

4. Barkai, N. & Leibler, S. Robustness in simple biochemical networks to transfer and process information. *Nature* **387**, 913–917 (1997).

5. Silva-Rocha, R. & de Lorenzo, V. Noise and Robustness in Prokaryotic Regulatory Networks. *Annu. Rev. Microbiol.* **64**, 257–275 (2010).

6. Stelling, J., Sauer, U., Szallasi, Z., Doyle, F. J. & Doyle, J. Robustness of Cellular Functions. *Cell* **118**, 675–685 (2004).

7. Eldar, A. *et al.* Robustness of the BMP morphogen gradient in Drosophila embryonic patterning. *Nature* **419**, 304–308 (2002).

8. Rao, C. V, Wolf, D. M. & Arkin, A. P. Control, exploitation and tolerance of intracellular noise. *Nature* **420**, 231–237 (2002).

9. Tsimring, L. S. Noise in biology. *Reports Prog. Phys.* **77**, (2014).

10. Raj, A. & van Oudenaarden, A. Nature, nurture, or chance: stochastic gene expression and its consequences. *Cell* **135**, 216–26 (2008).

11. Eldar, A. & Elowitz, M. B. Functional roles for noise in genetic circuits. *Nature* **467**, 167–173 (2010).

12. Balázsi, G., Van Oudenaarden, A. & Collins, J. J. Cellular decision making and biological noise: From microbes to mammals. *Cell* **144**, 910–925 (2011).

13. Wadhams, G. H. & Armitage, J. P. Making sense of it all: bacterial chemotaxis. *Nat.Rev.Mol.Cell Biol.* **5**, 1024–1037 (2004).

14. Shimizu, T. S., Tu, Y. & Berg, H. C. A modular gradient-sensing network for chemotaxis in Escherichia coli revealed by responses to time-varying stimuli. *Mol. Syst. Biol.* **6**, 1–14 (2010).

15. Lan, G., Schulmeister, S., Sourjik, V. & Tu, Y. Adapt locally and act globally: Strategy to maintain high chemoreceptor sensitivity in complex environments. *Mol. Syst. Biol.* **7**, 1–16 (2011).

16. Sourjik, V. & Wingreen, N. S. Responding to chemical gradients: bacterial chemotaxis. *Curr. Opin. Cell Biol.* **24**, 262–8 (2012).

17. Micali, G. & Endres, R. G. Bacterial chemotaxis: Information processing, thermodynamics, and behavior. *Curr. Opin. Microbiol.* **30**, 8–15 (2016).

18. Larsen, S. H., Reader, R. W., Kort, E. N., Tso, W. W. & Adler, J. Change in direction of flagellar rotation is the basis of the chemotactic response in Escherichia coli. *Nature* **249**, 74–77 (1974).

19. Macnab, R. M. & Ornston, M. K. Normal-to-curly flagellar transitions and their role in

bacterial tumbling. Stabilization of an alternative quaternary structure by mechanical force. *J. Mol. Biol.* **112**, 1–30 (1977).

20. Turner, L., Ryu, W. S. & Berg, H. C. Real-time imaging of fluorescent flagellar filaments. *J. Bacteriol.* **182**, 2793–2801 (2000).

21. Darnton, N. C., Turner, L., Rojevsky, S. & Berg, H. C. On torque and tumbling in swimming Escherichia coli. *J. Bacteriol.* **189**, 1756–1764 (2007).

22. Parkinson, J. S., Hazelbauer, G. L. & Falke, J. J. Signaling and sensory adaptation in Escherichia coli chemoreceptors: 2015 update. *Trends Microbiol.* **23**, 257–266 (2015).

23. Scharf, B. E., Fahrner, K. A., Turner, L. & Berg, H. C. Control of direction of flagellar rotation in bacterial chemotaxis. *Proc. Natl. Acad. Sci.* **95**, 201–206 (1998).

24. Alon, U. *et al.* Response regulator output in bacterial chemotaxis. *EMBO J.* **17**, 4238–4248 (1998).

25. Cluzel, P., Surette, M. & Leibler, S. An Ultrasensitive Bacterial Motor Revealed by Monitoring Signaling Proteins in Single Cells. *Science* **287**, 1652–1655 (2000).

26. Hess, J. F., Oosawa, K., Kaplan, N. & Simon, M. I. Phosphorylation of three proteins in the signaling pathway of bacterial chemotaxis. *Cell* **53**, 79–87 (1988).

27. Blat, Y. & Eisenbach, M. Phosphorylation-Dependent Binding of the Chemotaxis Signal Molecule CheY to Its Phosphatase, CheZ. *Biochemistry* **33**, 902–906 (1994).

28. Springer, M. S., Goy, M. F. & Adler, J. Protein methylation in behavioural control mechanisms and in signal transduction. *Nature* **280**, 279–284 (1979).

29. Kehry, M. R., Bond, M. W., Hunkapiller, M. W. & Dahlquist, F. W. Enzymatic deamidation of methyl-accepting chemotaxis proteins in Escherichia coli catalyzed by the cheB gene product. *Proc. Natl. Acad. Sci. U. S. A.* **80**, 3599–3603 (1983).

30. Borkovich, K. A., Alex, L. A. & Simon, M. I. Attenuation of sensory receptor signaling by covalent modification. *Proc. Natl. Acad. Sci.* **89**, 6756–6760 (1992).

31. Korobkova, E., Emonet, T., Vilar, J. M. G., Shimizu, T. S. & Cluzel, P. From molecular noise to behavioural variability in a single bacterium. *Nature* **428**, 574–578 (2004).

32. Colin, R., Rosazza, C., Vaknin, A. & Sourjik, V. Multiple sources of slow activity fluctuations in a bacterial chemosensory network. *Elife* **6**, 1–32 (2017).

33. Keegstra, J. M. *et al.* Phenotypic diversity and temporal variability in a bacterial signaling network revealed by single-cell FRET. *Elife* **6**, 1–33 (2017).

34. Matthäus, F., Jagodič, M. & Dobnikar, J. E. coli superdiffusion and chemotaxis-search strategy, precision, and motility. *Biophys. J.* **97**, 946–957 (2009).

35. Emonet, T. & Cluzel, P. Relationship between cellular response and behavioral variability in bacterial chemotaxis. *Proc. Natl. Acad. Sci. U. S. A.* **105**, 3304–3309 (2008).

36. He, R., Zhang, R. & Yuan, J. Noise-Induced Increase of Sensitivity in Bacterial Chemotaxis. *Biophys. J.* **111**, 430–437 (2016).

37. Flores, M., Shimizu, T. S., ten Wolde, P. R. & Tostevin, F. Signaling Noise Enhances Chemotactic Drift of E. coli. *Phys. Rev. Lett.* **109**, 148101 (2012).

38. Terasawa, S. *et al.* Coordinated reversal of flagellar motors on a single Escherichia coli cell. *Biophys. J.* **100**, 2193–2200 (2011).

39. Mears, P. J., Koirala, S., Rao, C. V., Golding, I. & Chemla, Y. R. Escherichia coli swimming is robust against variations in flagellar number. *Elife* **3**, 1–18 (2014).

40. Min, T. L. *et al.* High-resolution, long-term characterization of bacterial motility using optical tweezers. *Nat. Methods* **6**, 831–835 (2009).

41. Park, H. *et al.* Interdependence of behavioural variability and response to small stimuli in bacteria. *Nature* **468**, 819–821 (2010).

42. Min, T. L., Mears, P. J., Golding, I. & Chemla, Y. R. Chemotactic adaptation kinetics of individual Escherichia coli cells. *Proc. Natl. Acad. Sci.* **109**, 9869–9874 (2012).

43. Yuan, J. & Berg, H. C. Ultrasensitivity of an adaptive bacterial motor. *J. Mol. Biol.* **425**, 1760–

1764 (2013).

44. Li, M. & Hazelbauer, G. L. Cellular stoichiometries of the components of the chemotaxis signaling complex. *J. Bacteriol* **186**, 3687–3694 (2004).

45. Shamir, M., Bar-On, Y., Phillips, R. & Milo, R. SnapShot: Timescales in Cell Biology. *Cell* **164**, 1302-1302.e1 (2016).

46. Tu, Y. & Grinstein, G. How White Noise Generates Power-Law Switching in Bacterial Flagellar Motors. **208101**, 1–4 (2005).

47. Alon, U., Surette, M. G., Barkai, N. & Leibler, S. Robustness in bacterial chemotaxis. *Nature* **397**, 168–171 (1999).

48. Sourjik, V. & Berg, H. C. Receptor sensitivity in bacterial chemotaxis. *Proc. Natl. Acad. Sci. U. S. A.* **99**, 123–127 (2002).

49. Segall, J. E., Block, S. M. & Berg, H. C. Temporal comparisons in bacterial chemotaxis. *Proc. Natl. Acad. Sci. U. S. A.* **83**, 8987–8991 (1986).

50. Block, S. M., Segall, J. E. & Berg, H. C. Adaptation kinetics in bacterial chemotaxis. *J. Bacteriol.* **154**, 312–323 (1983).

51. Mesibov, R. & Adler, J. Chemotaxis toward amino-acids in Escherichia coli. *J. Bacteriol.* **112**, 315–326 (1972).

52. Mesibov, R., Ordal, G. W. & Adler, J. The range of attractant concentrations for bacterial chemotaxis and the threshold and size of response over this range. Weber law and related phenomena. *J. Gen. Physiol.* **62**, 203–223 (1973).

53. Vladimirov, N., Løvdok, L., Lebiedz, D. & Sourjik, V. Dependence of bacterial chemotaxis on gradient shape and adaptation rate. *PLoS Comput. Biol.* **4**, (2008).

54. Bitbol, A. F. & Wingreen, N. S. Fundamental constraints on the abundances of chemotaxis proteins. *Biophys. J.* **108**, 1293–1305 (2015).

55. Clausznitzer, D., Oleksiuk, O., Løvdok, L., Sourjik, V. & Endres, R. G. Chemotactic response

and adaptation dynamics in Escherichia coli. *PLoS Comput. Biol.* **6**, 1–11 (2010).

56. Mcquarrie, D. A. & Gillespie, D. T. Stochastic Theory and Simulations of Chemical Kinetics. *J. Appl. Probab.* **478**, 413–478 (1967).

57. Sourjik, V. & Berg, H. C. Binding of the Escherichia coli response regulator CheY to its target measured in vivo by fluorescence resonance energy transfer. *Proc. Natl. Acad. Sci. U. S. A.* **99**, 12669–12674 (2002).

58. Tindall, M. J., Porter, S. L., Wadhams, G. H., Maini, P. K. & Armitage, J. P. Spatiotemporal modelling of CheY complexes in Escherichia coli chemotaxis. *Prog. Biophys. Mol. Biol.* **100**, 40–46 (2009).

59. Paulsson, J. Summing up the noise in gene networks. *Nature* **427**, 415–8 (2004).

60. Paulsson, J. Models of stochastic gene expression. *Phys. Life Rev.* **2**, 157–175 (2005).

61. Golding, I., Paulsson, J., Zawilski, S. M. & Cox, E. C. Real-time kinetics of gene activity in individual bacteria. *Cell* **123**, 1025–1036 (2005).

62. Thattai, M. & van Oudenaarden, A. Intrinsic noise in gene regulatory networks. *Proc. Natl. Acad. Sci.* **98**, 8614–8619 (2001).

63. Yuan, J., Branch, R. W., Hosu, B. G. & Berg, H. C. Adaptation at the output of the chemotaxis signalling pathway. *Nature* **484**, 233–236 (2012).

64. Turner, L., Zhang, R., Darnton, N. C. & Berg, H. C. Visualization of flagella during bacterial swarming. *J. Bacteriol.* **192**, 3259–3267 (2010).

Figures

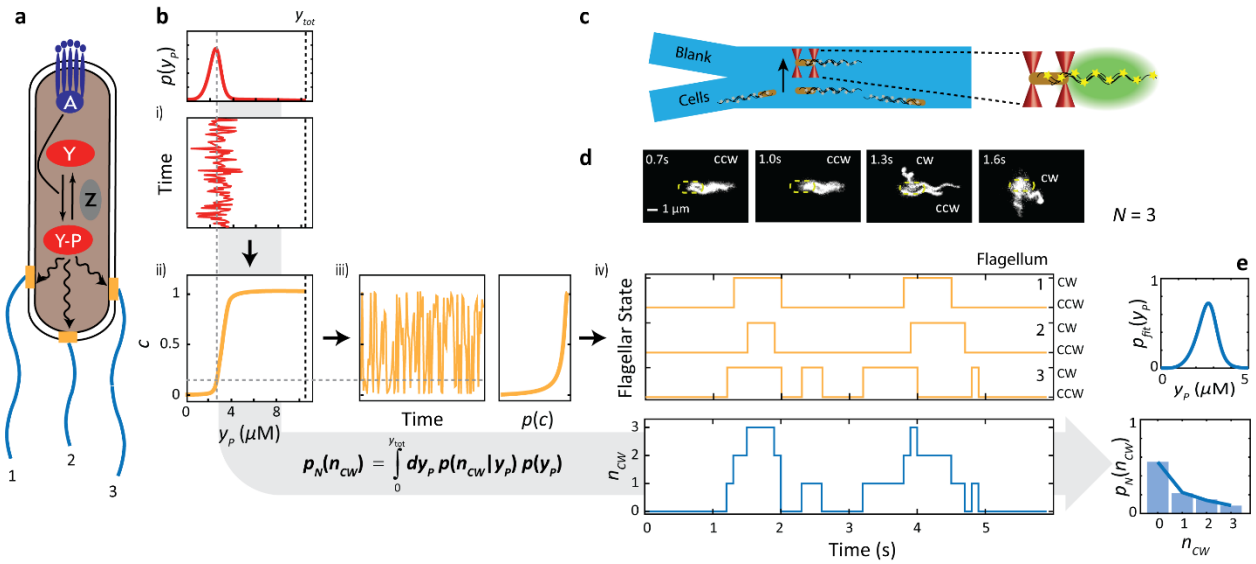

Figure 1. Estimating the temporal [CheY-P] distribution from flagellar dynamics of single *E. coli* cells. a. Schematic of a multi-flagellated *E. coli* cell showing key reactions of the chemotaxis signaling network. CheY is phosphorylated to CheY-P by the receptor kinase complex (CheA; dark blue); CheY-P is dephosphorylated by the phosphatase CheZ (gray). CheY-P binding to flagellar motors (mustard) causes a switch from CCW to CW rotation, which leads to cell tumbling. **b.** Temporal fluctuations in [CheY-P] due to chemotaxis network dynamics and their effect on flagellar switching statistics. i) [CheY-P] temporal fluctuations and corresponding distribution function $p(y_p)$. ii) Switch-like response of motor CW bias, c, to [CheY-P]. iii) Resulting temporal fluctuations in motor bias $c(t)$ and distribution of motor bias $p(c)$. iv) CCW/CW rotation state of three flagellar motors corresponding to the instantaneous motor bias c. The temporal [CheY-P] distribution function $p(y_P)$ is directly related to the probability distribution $p_N(n_{cw})$ that n_{cw} out of N flagella rotate CW through the integral Eq. (4) (large gray arrow). **c.** Schematic of two-channel

laminar flow chamber for optical trap assay. A single cell with fluorescently labelled flagella (gray stars) is captured from the bottom channel ("Cells"), aligned along the flow between two optical traps (red cones), moved to the upper channel ("Blank"), and its fluorescent flagella (yellow stars) imaged by stroboscopic slim-field microscopy (green). **d.** Fluorescence data trace from representative trapped cell with N = 3 flagella. Top, still images of fluorescent flagella, with position of the unlabeled cell body approximately indicated by the dashed yellow line. CW and CCW rotating flagella are labelled where clearly visible. Middle, CCW/CW rotation state of each flagellum vs. time (mustard). Bottom, corresponding number n_{cw} of CW flagella vs. time (light blue). **e**. Bottom, probability distribution $p_N(n_{cw})$, determined experimentally from d (light blue bars) and fit (solid blue line) based on the model in Eq. (4). Top, best fit estimate of the [CheY] probability distribution $p_{fit}(y_P)$.

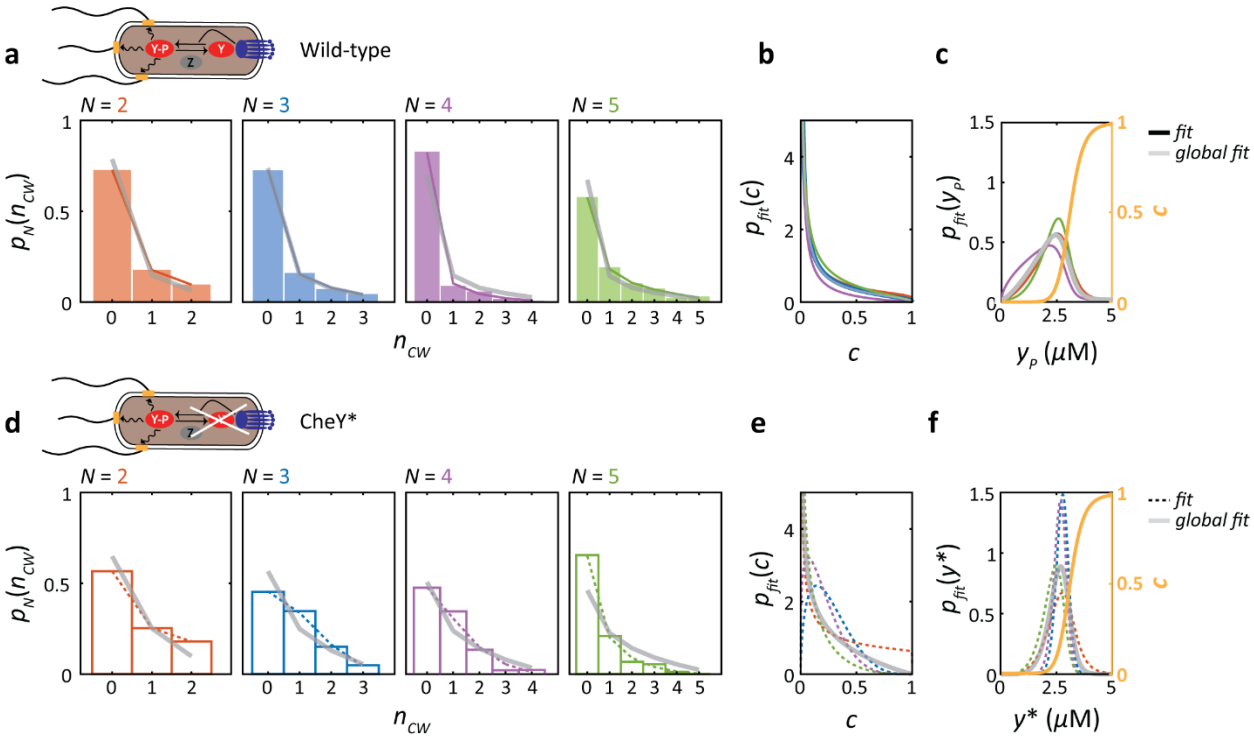

Figure 2. [CheY-P] fluctuations in the chemotaxis network at steady state. Measurement of flagellar dynamics and estimation of [CheY-P] fluctuations in wild-type *E. coli* strain HCB1660 (a-c) and in "CheY*" mutant strain PM87 expressing constitutively active CheY^{D13K} (d-f). **a.** Experimentally determined probability distribution $p_N(n_{cw})$ that n_{cw} out of N flagella rotate CW, grouped by cells with the same total number of flagella N = 2, 3, 4, 5 (number of cells = 13, 15, 14, 9 respectively). Best-fit distributions $p_{N,fit}(n_{cw})$ determined separately for each N (colored solid lines) as well as globally (gray solid lines) are overlaid with the observed distributions (colored filled bars). **b.** Best-fit probability distributions of the motor bias, $p_{fit}(c)$, determined separately for each N (colored solid curves) and globally (gray solid curve). **c.** Best fit probability distributions of [CheY-P], $p_{fit}(y_P)$, determined separately for each N (colored solid curves) and globally (gray solid curves). The motor bias c vs. y_P curve, Eq. (3), is overlaid for reference (mustard curve; right axis). **d-f.** Same as a-c for CheY* strain, showing experimental (open bars)

and best fit (dashed lines and curves) distributions, grouped by cells with the same total number of flagella N = 2, 3, 4, 5 (number of cells = 13, 13, 9, 9 respectively).

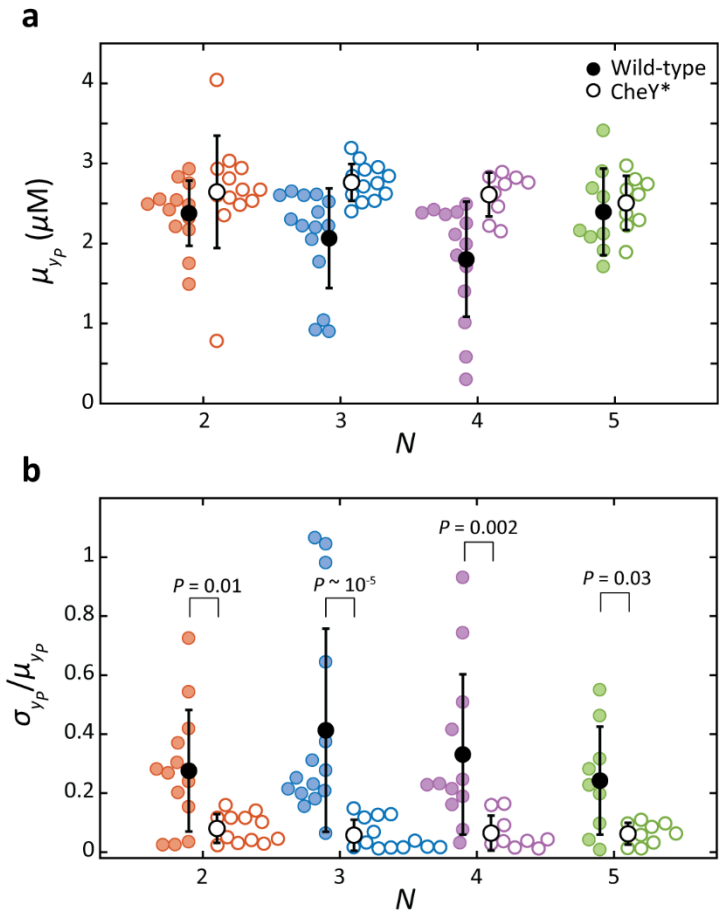

Figure 3. Estimate of the mean and coefficient of variation of [CheY-P] in individual cells at steady state. a. Comparison of mean [CheY-P], μ_{y_p}, determined for individual wild-type (colored circles) and CheY* cells (open circles), for different number of flagella *N*. **b.** Comparison of the coefficient of variation in [CheY-P], σ_{y_p}/μ_{y_p}, determined for individual wild-type (colored circles) and CheY* cells (open circles), for different *N*. Averages over each cell population are overlaid (black solid circles for wild-type, black open circles for CheY*); error bars represent standard deviation.

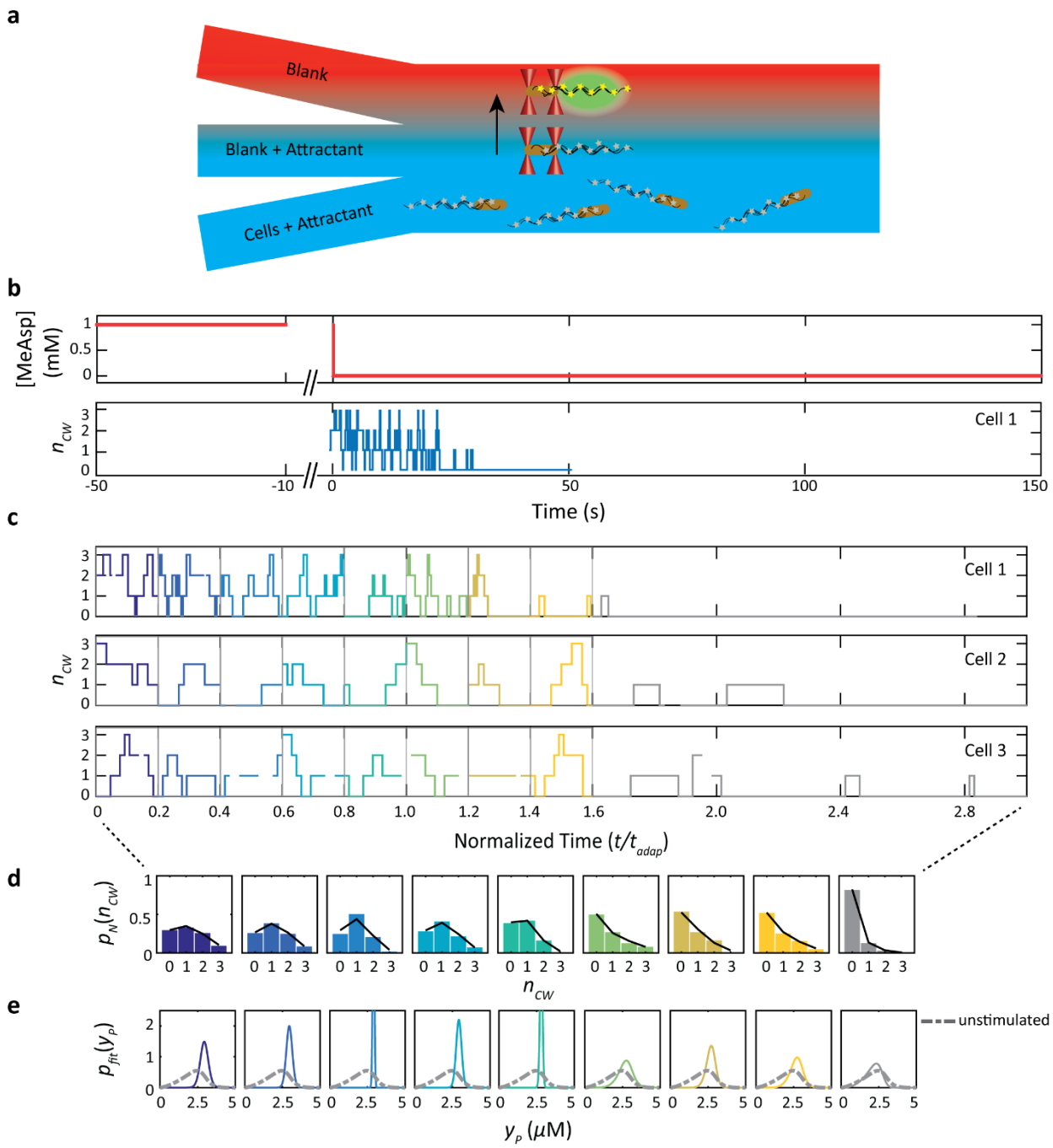

Figure 4. [CheY-P] fluctuations in the chemotaxis network upon stimulation. a. Schematic of three-channel laminar flow chamber for flagellar imaging of a cell experiencing a step down in attractant concentration. A single cell with fluorescently labelled flagella (gray stars) is captured from the bottom channel containing 1 mM MeAsp ("Cells + Attractant") and aligned along the

flow between two optical traps (red cones) in the middle channel ("Blank + attractant"). The trapped cell is then moved to the upper channel lacking MeAsp ("Blank") and its fluorescent flagella (yellow stars) are imaged (green). **b.** Representative trace showing the response of "Cell 1" to a step-down stimulus. Top, schematic of MeAsp concentration over time, showing the step down from 1 to 0 mM at $t = 0$. Data are not collected during the move from the middle to the top channel. Bottom, number n_{cw} of CW flagella over time after $t = 0$. **c-e.** Estimation of the [CheY-P] distribution in cells responding to a step-down stimulus. **c.** Traces from three representative "Cells 1, 2, 3" showing the number n_{cw} of CW flagella vs. time (normalized by each cell's adaptation time t_{adap}). Each trace is subdivided into windows of duration $0.2t_{adap}$, and data from each window is pooled across cells (for $N = 3$ flagella shown here, number of cells = 9). **d.** Distributions of the number of CW flagella $p_N(n_{cw})$ for each window (colored bars) with the calculated best fits (black solid lines). **e**. Best-fit [CheY-P] distributions, $p_{fit}(y_P)$, (colored curves) for each window. The [CheY-P] distribution for unstimulated cells is overlaid (gray dotted curve).

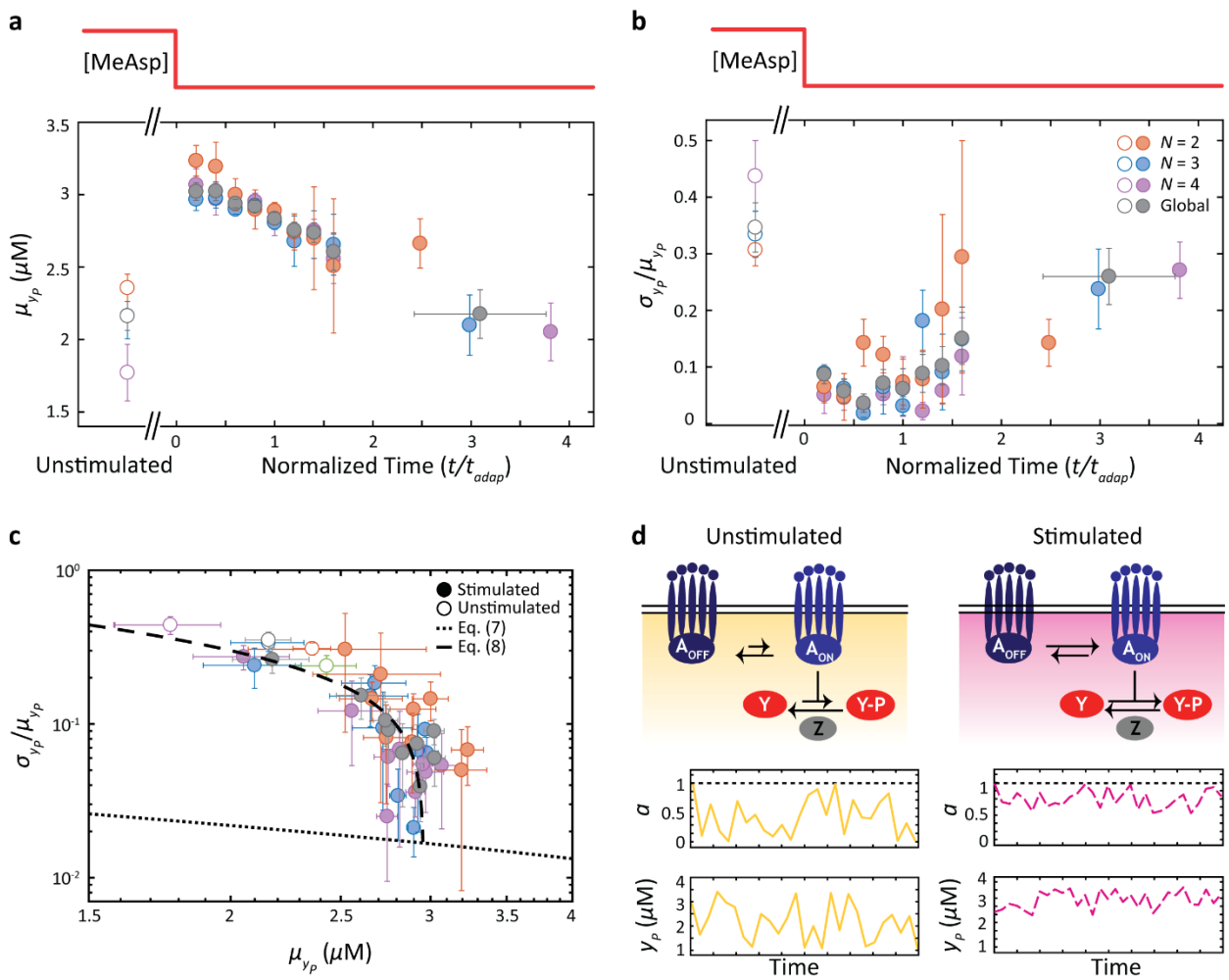

Figure 5. Reduction in [CheY-P] fluctuations upon network stimulation and model of network noise. a. Mean [CheY-P], μ_{y_p}, vs. normalized time t/t_{adap} after step down stimulus (top schematic, red) determined separately for each number of flagella N (colored filled circles) and globally (gray filled circles). **b.** Coefficient of variation in [CheY-P], σ_{y_p}/μ_{y_p}, after step down. Same color code as a. Data are pooled by cells with the same total number of flagella N = 2, 3, 4 (number of cells = 9, 9, 9). The pre-stimulus mean and coefficient of variation in [CheY-P] were obtained from the analysis of the unstimulated cells in Fig. 2 (open circles). **c.** Coefficient of variation in [CheY-P], σ_{y_p}/μ_{y_p}, vs. mean [CheY-P], μ_{y_p}, shown in **a** and **b** for stimulated (filled circles) and unstimulated (open circles) cells with N = 2, 3, 4 flagella (same color code as a). Comparison to models with

constant CheA activity, Eq. (7) (dotted line), and with fluctuating CheA activity, Eq. (8) (dashed line). **d.** Schematic of noise and kinetic ceiling in CheA activity, α, and their effects on CheY-P concentration fluctuations, y_P, in unstimulated (yellow) and stimulated (magenta) states of the cell.